



Bioadaptation of implants to In vitro and In vivo oxidative stress pathological conditions via nanotopography-induced FoxO1 signaling pathways to enhance Osteoimmunal regeneration

Jingyan Huang^{a,1}, Ruoqi Li^{a,1}, Jinghong Yang^a, Min Cai^a, Yichen Lee^a, Anxun Wang^{b,*}, Bin Cheng^{a,**}, Yan Wang^{a,***}

^a Hospital of Stomatology, Guanghua School of Stomatology, Sun Yat-sen University and Guangdong Key Laboratory of Stomatology, Guangzhou, Guangdong, 510055, China

^b The First Affiliated Hospital of Sun Yat-sen University, Guangzhou, Guangdong, 510080, China

ARTICLE INFO

Keywords:

Oxidative stress
Osteogenesis
TiO₂ nanotubes
FoxO1
Inflammation

ABSTRACT

Varieties of pathological conditions, including diabetes, are closely related to oxidative stress (OS), but the osseointegration or bioadaptation of implants to OS and the related mechanism remain poorly explored. In this study, the antioxidation and osteoimmune regeneration of titanium implants with micro/nanotopographies were evaluated under H₂O₂-, lipopolysaccharide (LPS)- and hyperglycemia-mediated cellular OS models and in diabetic rats as a representative animal model of OS. TiO₂ nanotube (TNT) coating on titanium implants directly induced superior osteogenic differentiation of bone mesenchymal stem cells (MSCs) and osseointegration compared with microscale sand blasted-acid etched topography (SLA) under OS, attributed to higher superoxide dismutase 2 activity, the neutralization of intracellular reactive oxygen species (ROS), and less apoptosis. Mechanistically, the oxidation resistance on TNT is driven by upregulated forkhead box transcription factor O1 (FoxO1), which is abolished after knockdown of FoxO1 via shRNA in MSCs. Indirectly, TNT also alleviates OS in macrophages, therefore inducing a higher portion of the M2 phenotype under OS with increased secretion of the anti-inflammatory cytokine IL-10, further promoting the osseointegration capacity compared with SLA. The current study not only suggests the potential application of TiO₂ nanotube-coated titanium implants in compromised conditions but also provides a systematic evaluation strategy for the future development of bone biomaterials.

1. Introduction

Although the survival rate of dental implants has been reported to be over 90% [1,2], compromised bone conditions endanger high success rates. The main concern is implicated in diabetes, cancer, aging and aging-related diseases such as osteoporosis, which can hamper bone healing around dental implants [2]. The methods for enhancing implant osseointegration under impaired bone conditions remain far from adequately developed [3]. To solve this problem, understanding the mechanism underlying impaired osseointegration in pathological

conditions is essential. Increasing research suggests that oxidative stress is a key etiology of a number of the pathological conditions listed above [4–8]. Consequently, exploring the mechanisms of osseointegration and bioadaptation of implants to oxidative stress becomes the path leading to precisely-promoted performance of implants under pathological conditions.

Currently, oxidative stress is defined as an imbalance between oxidants and antioxidants in favor of oxidants, leading to a disruption of redox signaling and control and/or molecular damage [9]. As an etiological factor of many pathological conditions, oxidative stress also

Peer review under responsibility of KeAi Communications Co., Ltd.

* Corresponding author.

** Corresponding author..

*** Corresponding author.

E-mail addresses: wanganx@mail.sysu.edu.cn (A. Wang), chengbin@mail.sysu.edu.cn (B. Cheng), wangyan9@mail.sysu.edu.cn (Y. Wang).

¹ Authors contributed equally to the work.

<https://doi.org/10.1016/j.bioactmat.2021.02.023>

Received 4 November 2020; Received in revised form 16 February 2021; Accepted 18 February 2021

2452-199X/© 2021 The Authors. Publishing services by Elsevier B.V. on behalf of KeAi Communications Co. Ltd. This is an open access article under the CC

BY-NC-ND license (<http://creativecommons.org/licenses/by-nc-nd/4.0/>).

plays critical roles in inflammation, fibrosis and healing, which are the major events occurring during the implantation of biomaterials [10]. Oxidative stress can inhibit the proliferation of osteoblasts and disequilibrate the osteogenic/adipogenic differentiation balance of MSCs around biomaterials by modulating the PPAR γ and Wnt pathways [11]. In addition, self-defense by elevating detoxification/antioxidant potential to scavenge ROS has been developed to promote survival [8]. Among the many mechanisms, the forkhead box transcription factor (FOXO) family of transcription factors is critical, playing essential roles in many biological processes, including cellular proliferation, apoptosis and differentiation [12]. In addition, a bidirectional effect of FOXOs on balancing osteogenic differentiation has been discovered in bone mesenchymal stem cells (BMSCs) [13]. The cell- and stage-specific effects warrant further exploration of the role of the foxO family under oxidative stress in the microenvironment surrounding biomaterials.

Immunity has been found to play important roles during wound healing and osteogenesis around bone implant biomaterials. Immune cells participate actively in bone physiology and pathology by releasing regulatory molecules that elicit significant effects on osteoclastogenesis and osteogenesis. Macrophages, as plastic effector cells in innate and adaptive immunity, can respond to various biophysical and biochemical cues from bone biomaterials and immunomodulate osteogenesis via varied polarization and secreted inflammatory cytokines [14]. Zetao Chen et al. found that tuning the surface chemistry and scale of the nanotopography significantly modulated the osteoimmune environment, including altered expression of inflammatory cytokines, along with osteogenic, angiogenic, and fibrogenic factors. The generated osteoimmune environment significantly affected the osteogenic differentiation of bone marrow stromal cells, implying the potential of nanoengineered surfaces for the development of advanced bone biomaterials with favorable osteoimmunomodulatory properties [15]. However, most of the research was conducted under physiological conditions, exploring the effect of inflammation induced by the implantation of bone biomaterials in the later stages of surrounding bone formation and wound healing. However, little is known about the immunoregulatory effect of macrophages on the osteogenesis of biomaterials under compromised bone conditions with innate oxidative stress.

Whether the surface topography of dental implants can modulate the cellular response and further osseointegration has been well explored. Our previous study showed that compared with common commercial microscale sand blasted-acid etched topography (SLA), nanoscale TiO₂ nanotube (TNT) topography enhanced the osseointegration of titanium implants under both normal conditions and high glucose-induced oxidative stress [16,17]. To determine the osteogenic mechanism of TNT under oxidative stress, the antioxidant and osteogenic capacities of mesenchymal stem cells (MSCs) on different micro/nanotopographies under H₂O₂, lipopolysaccharide (LPS)- and hyperglycemia-mediated models of oxidative stress were evaluated, as was the osseointegration performance in diabetic rats. Furthermore, the immune responses of macrophages, including polarization and secreted inflammatory cytokines, were also evaluated under oxidative stress. Mechanistically, the effects of FoxO1 on oxidation resistance, inflammation and bone formation in TNTs under oxidative stress were also elucidated by measuring the expression of signaling factors and silencing FoxO1 in MSCs. Finally, the crosstalk between MSCs and macrophages (M ϕ s) on TNTs under oxidative stress was explored, and the orchestrated effect on osseointegration was further verified in diabetic rats. This study is expected to deepen the understanding of the osteogenic mechanism of Ti implants under oxidative stress and to lay a theoretical foundation for developing novel surface treatments to enhance implant osseointegration under pathological conditions.

2. Materials and methods

Material preparation and surface characterization of different titanium

surfaces: Pure Ti foils (diameter: 10 mm, thickness: 0.6 mm, Baoji Titanium Industry, China) were used as the culture substrate, and cylinder-shaped pure Ti implants (diameter: 2 mm, length: 4 mm, Foshan Anchi Biotechnology Industry, Foshan, China) were used for animal experiments. The Ti samples were grouped according to three surface treatments, including sandblasted and acid-etched Ti (SLA) and TiO₂ nanotubes (TNTs), as previously reported [16]. Briefly, the Ti foils were polished and then ultrasonically cleaned. SLA surfaces were further blasted with silicon dioxide particles (particle size: 106–150 μ m) and then acid-etched using 10% HCl:10% H₂SO₄ (1:1, v/v) at 60 °C for 30 min. TNT surfaces were prepared by anodizing in aqueous electrolyte at 20 V for 30 min. Then, the specimens were sterilized in an autoclave for bioactivity evaluation. The topography of Ti discs sputter-coated with gold was observed by scanning electron microscopy (SEM: LEO1530VPFESEM, Zeiss, Germany). The crystalline phases were identified by an X-ray diffractometer (ESCALab250, ESCA, USA) in θ -2 θ geometry using Cu K α radiation. The surface roughness was measured using a laser scanning confocal microscope profilometer (LSM700, Zeiss, Germany) with the parameters Sa (the arithmetic average of the 3D roughness) and Sq (the quadratic average of the 3D roughness). The hydrophilicity of the titanium surfaces was evaluated by determining the contact angles using a contact angle analyzer (OCA15, Dataphysics, Germany).

Cell culture: BMSCs were harvested from 3-week-old female C57BL/6 mice as previously described [18]. Briefly, the femurs and tibiae were separated and flushed to remove bone marrow. Then, the compact bones were fragmented into small pieces, digested with 1 mg/mL collagenase type I and seeded into cell culture flasks in a humidified atmosphere with 5% CO₂ at 37 °C. At approximately 80% confluence, the MSCs were trypsinized and subcultured. The cells at passages 3–5 were used in the following experiments. To simulate various conditions of oxidative stress, 300 μ M H₂O₂, 1 μ g/mL lipopolysaccharide (LPS), or 22 mM glucose was added to the culture medium according to pilot and previous studies [15,17], while cells were also cultured in normal medium with a glucose concentration of 5.5 mM as a control. Additionally, basic osteogenic differentiation medium (Cyagen Co.) was further used to culture MSCs for differentiation assays.

To knock down FoxO1, MSCs were transfected with a vector containing FoxO1 shRNA lentiviral particles following the manufacturer's protocol (Cyagen Co., USA). Stable clones were selected and named shFoxO1, while an empty vector was also transfected as a negative control and named shControl. Lentiviral particles were designed and synthesized by Cyagen Co. (USA), and their sequences are listed in Table S1.

A RAW264.7 (M ϕ , a murine-derived macrophage cell line kindly provided by the Institute of Biochemistry and Cell Biology, Chinese Academy of Sciences, Shanghai, China) cell culture was maintained in low-glucose DMEM (Life Technologies) according to a standard protocol [15] and was treated with the same stimulation as MSCs.

ROS production in MSCs and M ϕ s adhered to Ti surfaces under oxidative stress: To evaluate the levels of oxidative stress modulated by the 2 Ti surfaces, the endogenous ROS in MSCs and M ϕ s on the substrates were quantified with an oxygen radical-sensitive probe, DCFH-DA staining (Beyotime, China). Briefly, MSCs/M ϕ s adhered to different substrates were treated with oxidative stress inducers for 24 h. Then, the cells were washed with PBS and incubated with 5 μ M DCFH-DA for 30 min. Relative fluorescent intensities were quantified using a flow cytometer (excitation and emission filters of 488 and 530 nm) (Becton Dickinson, USA).

Antioxidation capacity, adhesion, proliferation and osteogenic differentiation of MSCs on Ti surfaces under H₂O₂-induced oxidative stress: To determine how ROS production was regulated by the redox control induced by Ti surfaces under oxidative stress, the activity of antioxidant enzymes was measured under stimulation with the model inducer H₂O₂. After treatment with H₂O₂ for 24 h, MSCs/M ϕ s on different substrates were lysed. Subsequently, the supernatant was used for determination of

superoxide dismutase (SOD)/catalase (CAT) activity using a SOD/CAT assay kit (Beyotime, China) according to the manufacturer's instructions.

To evaluate oxidative stress damage, cell viability and apoptosis were measured. Cell viability after treatment with the indicated oxidative stress inducers at the indicated times was evaluated to establish an oxidative stress model using a cell counting kit-8 (CCK-8) (Fluka, MO, USA) according to the manufacturer's instructions. For apoptosis evaluation, all digested cells on Ti surfaces after treatment with H₂O₂ for 24 h were stained with Annexin V-FITC and PI according to the instructions provided with a commercial apoptosis detection kit (Beyotime, China).

To evaluate the effect of oxidative stress on the adhesion of MSCs, the organization of actin filaments of adherent cells on the 2 substrates was evaluated by immunofluorescence staining with F-actin (red fluorescence, Solarbio, China) at 24 h of culture. After counterstaining with DAPI, MSCs were observed by confocal laser scanning microscopy (CLSM: LSM780, Zeiss, Germany). The proliferation of MSCs on the 2 substrates was also measured using the CCK-8 kit at culture times of days 1 and 3 with/without H₂O₂ stimulation.

To investigate the effect of oxidative stress on the osteogenic capacity of MSCs on Ti surfaces, markers of osteogenic differentiation, including ALP viability and mineralization levels, were measured. MSCs were cultured onto 2 substrates in osteogenic differentiation medium with/without stimulators (H₂O₂/LPS). On day 7, the ALP activity was measured using an ALP kit (Jiancheng, Nanjing, China) and was then normalized to the total protein amount measured by BCA Protein Assay (Beyotime, China). Extracellular matrix (ECM) mineralization of MSCs after incubation for 21 days was assessed by Alizarin Red staining. After fixing with 4% paraformaldehyde, the constructs were stained using Alizarin Red (Cyagens). Thereafter, the stain on the specimens was imaged by scanning electron microscopy (M205A, Leica, Germany) and then dissolved in 10% cetylpyridinium chloride (Sigma, USA) for semiquantitative analysis.

Effect of FoxO1 silencing on the oxidation resistance and osteogenic superiority of MSCs on TNT under oxidative stress: To reveal the molecular mechanism of antioxidation on TNT, the expression levels of typical signaling proteins in MSCs were measured by Western blot. After the cells on 2 Ti surfaces were cultured with/without H₂O₂ for 24 h, the protein was extracted using RIPA buffer, resolved by SDS–polyacrylamide gels and then transferred to PVDF membranes. Primary antibodies against FoxO1 (2880), LC3I/II (12741S), CAT (12980S), SOD2 (13141S) and GAPDH (97166S) from CST (USA) were used. Peroxidase-conjugated secondary antibodies (7074&7076) from CST were used, and the antigen-antibody reaction was visualized by enhanced chemiluminescence assay (ECL, Thermo).

To elaborate the contribution of FoxO1 to the oxidation resistance and osteogenic superiority of MSCs in TNT under oxidative stress, the transcription factor FoxO1 was silenced using a shRNA lentiviral vector. Thereafter, ROS production, apoptosis, and ALP activity were measured in shFoxO1 and shControl MSCs on 2 Ti surfaces under H₂O₂-induced oxidative stress. In the quantitation of apoptosis using a commercial apoptosis detection kit (Multi Sciences, China), Annexin V+/7-AAD-populations were considered early apoptotic, whereas double-positive (Annexin V+/7-AAD+) cells were considered late apoptotic, and the sum of these two populations was considered total apoptosis. In addition, the expression levels of FoxO1, SOD2, OPN, RUNX2, and β-actin were also evaluated by Western blot with additional primary antibodies against OPN (8448) and RUNX2 (23981) from Abcam (UK) and β-actin from Sigma (3854, USA).

The inflammatory response on Ti surfaces under oxidative stress: To determine how Mφs on Ti surfaces survived redox regulation under H₂O₂-mediated oxidative stress, the expression of antioxidant enzymes was measured in Mφs parallel to MSCs.

As oxidative stress is closely related to inflammation, the polarization of macrophages was also evaluated using immunofluorescence. RAW264.7 cells were seeded onto the Ti surface with 2 topographies in

24-well plates (2 × 10⁵ cells/well). Following adhesion overnight, cells were stimulated with 300 μM H₂O₂, 1 μg/mL LPS or 22 mM glucose for 24 h. After fixation in 4% paraformaldehyde for 20 min and permeabilization with 0.1% Triton X-100 for 10 min, the cells were blocked with 1% bovine serum albumin (BSA) in PBS for 30 min at ambient temperature. Then, the cells were incubated with primary antibodies specific for rabbit-anti-mouse iNOS (1:100 in 1% BSA, Abcam) and mouse-anti-mouse CD163 (1:100 in 1% BSA, Santa Cruz) overnight at 4 °C. Then, incubation with Alexa Fluor-conjugated secondary antibodies (1:500 in 1% BSA, Abcam & Cell Signaling Technology) was carried out for 1 h at room temperature. DAPI was then used to counterstain the nuclei before the samples were imaged with a confocal laser scanning microscope (Olympus). All samples were analyzed in triplicate, and fluorescence intensities were quantitatively analyzed using NIH ImageJ software [19].

Additionally, the expression of inflammatory cytokines was detected by cytokine microarray and qPCR. For the H₂O₂- and LPS-induced models, supernatants from RAW264.7 cells and MSCs cultured on different surfaces under normal, H₂O₂-derived oxidative stress and LPS-derived inflammatory conditions were collected for cytokine protein level detection via Meso Scale Discovery (MSD) technology using a V-PLEX Proinflammatory Panel 1 (mouse) Multiplex Assay (K15048D). A MESO QuickPlex SQ 120 machine and MSD Discovery Workbench software version 4.0.12 were used for the detection and data analyses, respectively. A series of isochronal maps reflecting the concentrations of the cytokines were constructed using GraphPad Prism software 8 (GraphPad Software Inc., San Diego, CA, USA). For the hyperglycemia-induced model, the mRNA expression levels of inflammatory cytokines, including TNF-α, iNOS and IL-10, from macrophages on 2 Ti surfaces under hyperglycemia were measured by qPCR. Briefly, total RNA was isolated from cells using an RNA-Quick Purification Kit (Yishan, Shanghai, China) following the manufacturer's protocol. The sequences of the primers used for PCR are provided in Table S2. Data were collected and analyzed with a Quantstudio 5 Instrument (ABI).

Particularly to evaluate the effect of the classic stimulator LPS on the shape of RAW264.7 cells, the morphology of RAW cells was measured on the model substrate TNT. RAW cells were plated on the TNT surface at a density of 10⁴/mL. After overnight growth, 1 μg/mL LPS was added to activate inflammatory macrophages for 12 h. Subsequently, the cells were fixed in 4% paraformaldehyde for confocal microscopy and SEM observation. Meanwhile, the expression of iNOS and CD163 in Mφs stimulated with LPS on TNTs was measured by immunofluorescence, and the mRNA expression levels of M1 macrophage markers (CD86, iNOS, TNF-α, IL-18) and M2 macrophage markers (CD206, IL-10) were measured by qPCR.

Crosstalk between MSCs and Mφs on TNTs under oxidative stress: To investigate the effect of nanotopography-dependent osteoimmunity on the osteogenic differentiation of BMSCs under oxidative stress, the supernatants from RAW264.7 cells cultured on the 2 surfaces stimulated with H₂O₂ were harvested and then diluted 1:1 in H₂O₂-supplemented complete BMSC culture medium (Fig. 7A). In this conditioned medium, MSCs were cultured for 7 and 21 d to evaluate ALP activity and ECM mineralization, respectively. To further determine the osteoimmunity regulation of Mφs to MSCs on TNTs specifically, supernatants from H₂O₂-treated Mφs were mixed with complete culture medium with/without H₂O₂, denoted H₂O₂+CM_{H2O2} and CM_{H2O2}, respectively. The ALP activity and ECM mineralization of MSCs in such conditions were compared to normally cultured (control) and H₂O₂-stimulated MSCs (H₂O₂) (Fig. 7D). Similar treatments were adopted in the LPS-mediated model, named control, LPS, CM and LPS + CM. Then, the osteogenic capacity of MSCs was evaluated in the same way.

To explore the immunoregulation of MSCs on the inflammatory response of Mφs in turn, coculture was performed (Fig. 6E) by seeding RAW264.7 cells on TNT substrate in the lower chamber and BMSCs in the upper chamber of a 24-well Transwell apparatus with a 0.4-μm pore size (Corning, USA) at a ratio of 10:1. For the Co-control group, H₂O₂-

treated Mφs were cocultured with MSCs under normal conditions, while for the Co-H₂O₂ group, cocultured MSCs and Mφs were both stimulated with H₂O₂. RAW264.7 cells in normal or H₂O₂-containing medium alone were used as the control or H₂O₂ groups. After culture for 24 h, the supernatants of RAW264.7 cells from the 4 groups were collected to analyze the secreted inflammatory cytokines using the MSD mentioned above.

Oxidative stress, inflammatory response and osteointegration of implants in diabetic rats: Eighty-four male Sprague–Dawley (SD) rats weighing 220–250 g were purchased from the Guangdong Medical Laboratory Animal Center (Foshan, China) and were used in the animal experiment. The experiment was approved by the Institutional Animal Care and Use Committee of Sun Yat-sen University (Approval No. SYSU-IACUC-2019-000261) and was conducted according to the ARRIVE guidelines [20] and the U.K. Animals (Scientific Procedures) Act [21].

The rats were divided into 2 groups. One group of rats received intraperitoneal (i.p.) injection of streptozotocin (52 mg/kg; MP Biomedicals, USA) to establish a diabetic rat model (DM), while an equal volume of citrate buffer was injected into the other group as a control. After 7 days, random blood glucose (RBS) was monitored from a tail vein blood sample using a glucometer (Johnson, USA) on the 5th day after the injection. Eventually, 24 rats with RBS higher than 300 mg/dL were selected for the DM model [17]. To verify diabetic rats as an animal model of oxidative stress, 24-h urine samples were collected from each rat using a metabolic cage, and blood samples were collected from the tail veins for serum measurements. After centrifugation for 15 min at 3000 rpm, the obtained serum and urine samples were used to measure malondialdehyde (MDA) levels and 8-hydroxydeoxyguanosine (8-OHdG), respectively, using an MDA detection kit (Yeyuan, Shanghai, China) and an ELISA kit (MSKBIO, Wuhan, China).

According to the procedure in our previous study [16], the distal end of the rat femur was surgically exposed, and Ti implants with 2 modified surfaces were randomly implanted in each femur after anesthesia with 3% Nembutal (30 mg kg⁻¹). After healing for 7 days and 1 and 2 months, 16 rats were sacrificed, and femurs with Ti implants were harvested and stored in 4% paraformaldehyde for further evaluation.

To analyze the oxidative stress in the peri-implant bone tissue, immunohistochemistry staining was performed on the specimens harvested on day 7 with antibodies specific for 4-hydroxy-2-nonenal (4-HNE, 1:100 dilution, bs-6313R), one of the most specific lipid peroxidation products, along with 8-OHdG (1:200 dilution, bs-1278R) [22]. Furthermore, the early immune response around the implants was evaluated by analyzing the expression of inflammatory cytokines in specimens harvested on day 7 using antibodies specific for TNF-α (1:200 dilution, bs-10802R) and IL-10 (1:200 dilution, bs-6761R) [23]. Then, the sections were scanned by histomorphometric examination using a ScanScope XT tissue slide scanner (Aperio, Leica Biosystems, Buffalo Grove, IL, USA).

To evaluate the osseointegration level of implants, histological analysis was performed. Specimens harvested at weeks 4 and 8 were dehydrated and embedded in methylmethacrylate without decalcification. Thirty-micron-thick serial sections were obtained by a diamond blade along the long axis of the implants, stained with Van Gieson's (VG) picrofuchsin and observed under light microscopy (BX51, Olympus, Tokyo, Japan) for histomorphometric analysis. The percentage of bone–implant contact (BIC%) was calculated using the Image-Pro Plus 6.0 image analysis system.

Statistical analysis: All data are presented as the means ± standard deviation (SD). Statistical analysis was performed with SPSS 25.0 statistical software (SPSS Inc., Chicago, IL) via pair-grouped Student's *t*-test, independent *t*-test and one-way analysis of variance (ANOVA). The confidence levels were set at 95%.

3. Results

3.1. Cellular models of oxidative stress formulated by H₂O₂, LPS and high glucose

To establish a classic model of oxidative stress, H₂O₂ at crescent concentrations ranging from 100–1000 μM was applied to stimulate cells. The results showed that after treatment for 24 h, the cell viability decreased as the concentration of H₂O₂ increased (Fig. S1A). In addition, under stimulation with 300 μM H₂O₂, cellular viability began to decrease significantly with significantly increased intracellular ROS (Fig. 1A). Conversely, H₂O₂ at a concentration of 300 μM increased intracellular ROS production (Fig. 1B) and significantly decreased the viability of macrophages (Fig. S1B). Thus, 300 μM H₂O₂ was selected to establish the classic cellular model of oxidative stress and was applied in the following experiments.

To explore the pattern of inflammation-induced oxidative stress, LPS was utilized. LPS (1 μg/mL) significantly increased intracellular ROS in Mφs and slightly suppressed cell viability (Fig. 1D&S1D). In contrast, the increase in ROS in MSCs after LPS stimulation showed no significant difference (Fig. 1C) despite the significantly reduced viability (Fig. S1C). However, ROS production in MSCs was significantly exaggerated in conditioned medium from Mφs (Fig. 1C). These results indicated that LPS can initiate oxidative stress in macrophages, which further activates ROS production in MSCs.

Specifically, to simulate diabetes-related oxidative stress *ex vivo*, high glucose was adopted. Similar to our previous study [17], high glucose (22 mM) also triggered increased ROS (Fig. 1E) and statistically inhibited the viability of MSCs on day 3 (Fig. S1E). For Mφs, high glucose also induced a slight increase in ROS (Fig. 1F) despite the increased cell viability (Fig. S1F). Thus, high glucose (22 mM) was used as another inducer of cellular oxidative stress.

3.2. TNT restrained oxidative stress in MSCs and Mφ

As shown in Fig. S2 and our previous report [16], the surface of TNT was characterized by evenly distributed nanotubes with an inner diameter of approximately 80 nm and a length of approximately 500 nm, while SLA presented pits and crater-like holes of several micrometers (Fig. S2A). The XRD patterns in Fig. S2B revealed that TNT and SLA consisted of titanium in amorphous form, without anatase or rutile TiO₂. The roughness, including Sa and Sq, of TNTs was significantly lower than that of SLAs (Fig. S2C&D). Fig. S2E shows that the average contact angle of TNT was approximately 8.4°, which was significantly lower than that of SLA (approximately 94.1°), indicating the superior hydrophilicity of TNT.

To investigate the antioxidant capacity of the two micro/nanotopographies, endogenous ROS production in MSCs was measured. After exposure to either 300 μM H₂O₂ or 1 μg/mL LPS for 1 h and 12 h, respectively, the endogenous ROS production on the 2 surfaces increased significantly; in particular, on SLA, the value almost doubled and was higher than that on TNT (Fig. 2A&B). Additionally, similar to the response of osteoblasts in our previous study [17], high-glucose conditions induced excess intracellular ROS levels in MSCs, but the TNT surface relieved oxidative stress compared with SLA (Fig. 2C).

For macrophages, after treatment with H₂O₂, LPS and high glucose, the ROS levels of RAW264.7 cells on both types of Ti surfaces increased significantly (*p* < 0.05). However, ROS production in TNTs was still lower than that in SLAs (Fig. 2D–F), consistent with MSCs. Collectively, TNT restrained oxidative stress in MSCs and Mφs compared with SLA.

3.3. TNT enhanced oxidation resistance and osteogenic differentiation of MSCs under oxidative stress

To determine how ROS production was regulated by the redox reaction after H₂O₂ stimulation, the activity of antioxidant enzymes was

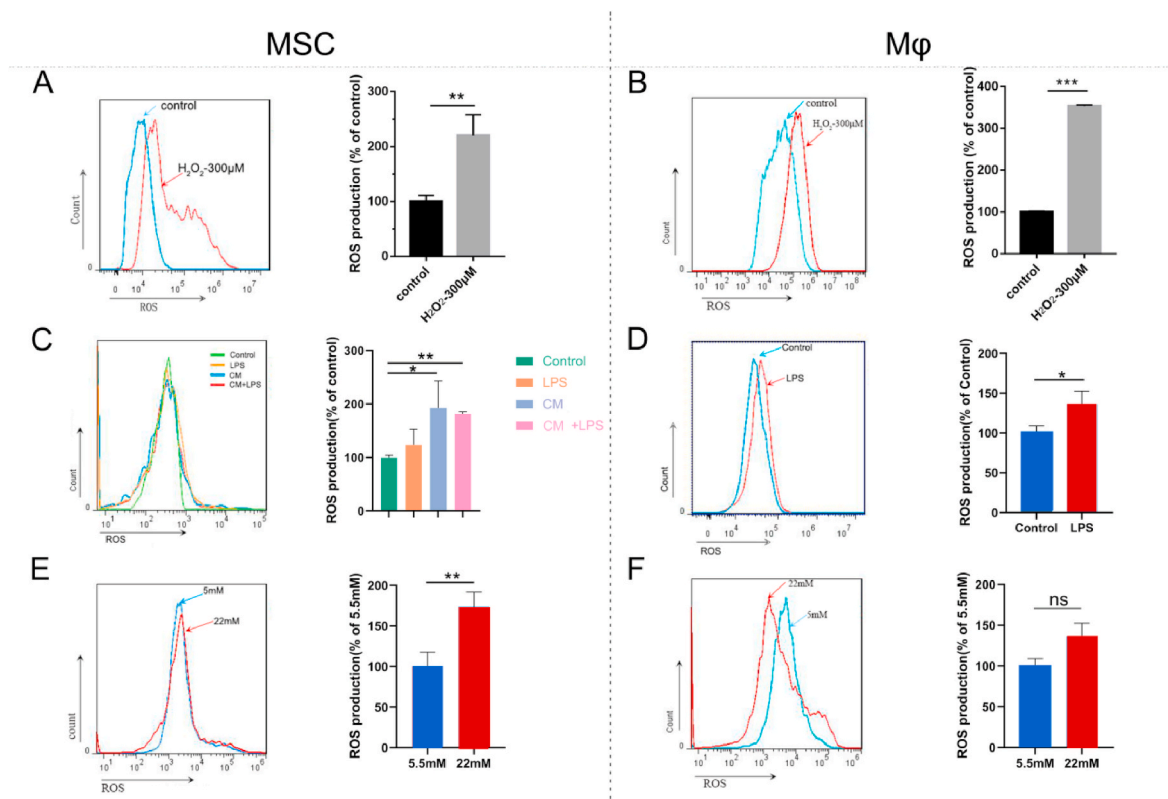


Fig. 1. Cellular models of oxidative stress formulated by H_2O_2 , LPS and high glucose. The effects of 300 μ M H_2O_2 , 1 μ g/mL LPS and high glucose (22 mM) on intracellular production of ROS in MSCs (A, C, E) and Mφs (B, D, F). Coculture of MSCs with conditioned medium (CM) from LPS-treated Mφs indicated that macrophages amplified LPS-mediated upregulation of ROS in MSCs (C). Control: culture media without extra stimulation, LPS: LPS (1 μ g/mL)-supplemented media, CM: conditioned media from LPS-treated Mφs, LPS + CM: conditioned media from LPS-treated Mφs mixed with extra LPS. $*p < 0.05$, $**p < 0.01$, $***p < 0.001$. ns indicates no significant difference.

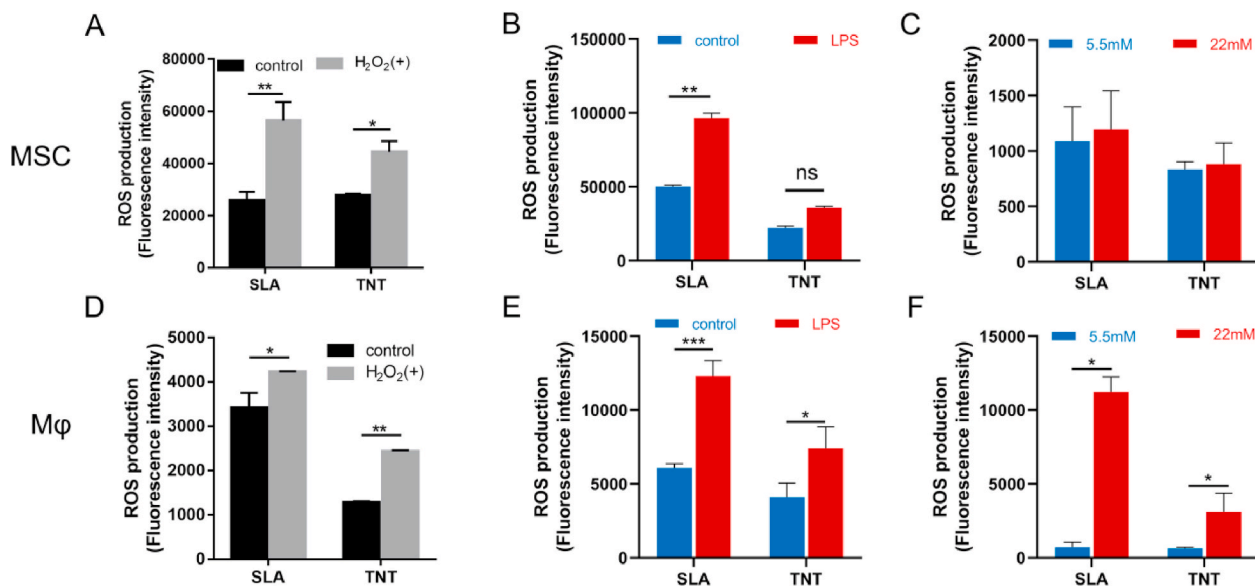


Fig. 2. TNT restrained oxidative stress in MSCs and Mφ. Intracellular ROS production of MSCs (A–C) and Mφs (D–F) on SLA and TNT under H_2O_2 -, LPS-, and hyperglycemia-mediated oxidative stress. $*p < 0.05$, $**p < 0.01$, $***p < 0.001$. ns indicates no significant difference.

measured. The SOD activity of MSCs on TNT was promoted to a level higher than SLA ($p < 0.01$) after stimulation with H_2O_2 . In comparison, the SOD activity of MSCs was inhibited on SLA. Similarly, the CAT activity of MSCs on 2 surfaces was consumed ($p < 0.01$), to neutralize the oxidation stress from H_2O_2 (Fig. 3A&B). The results indicated that TNT

induced oxidation resistance by elevating SOD.

To evaluate oxidative stress damage, cell apoptosis was measured. Under normal conditions, fewer apoptotic MSCs were detected on TNTs. After exposure to H_2O_2 for 1 d, the apoptosis incidence climbed significantly to comparable levels on the 2 Ti surfaces (Fig. 3C).

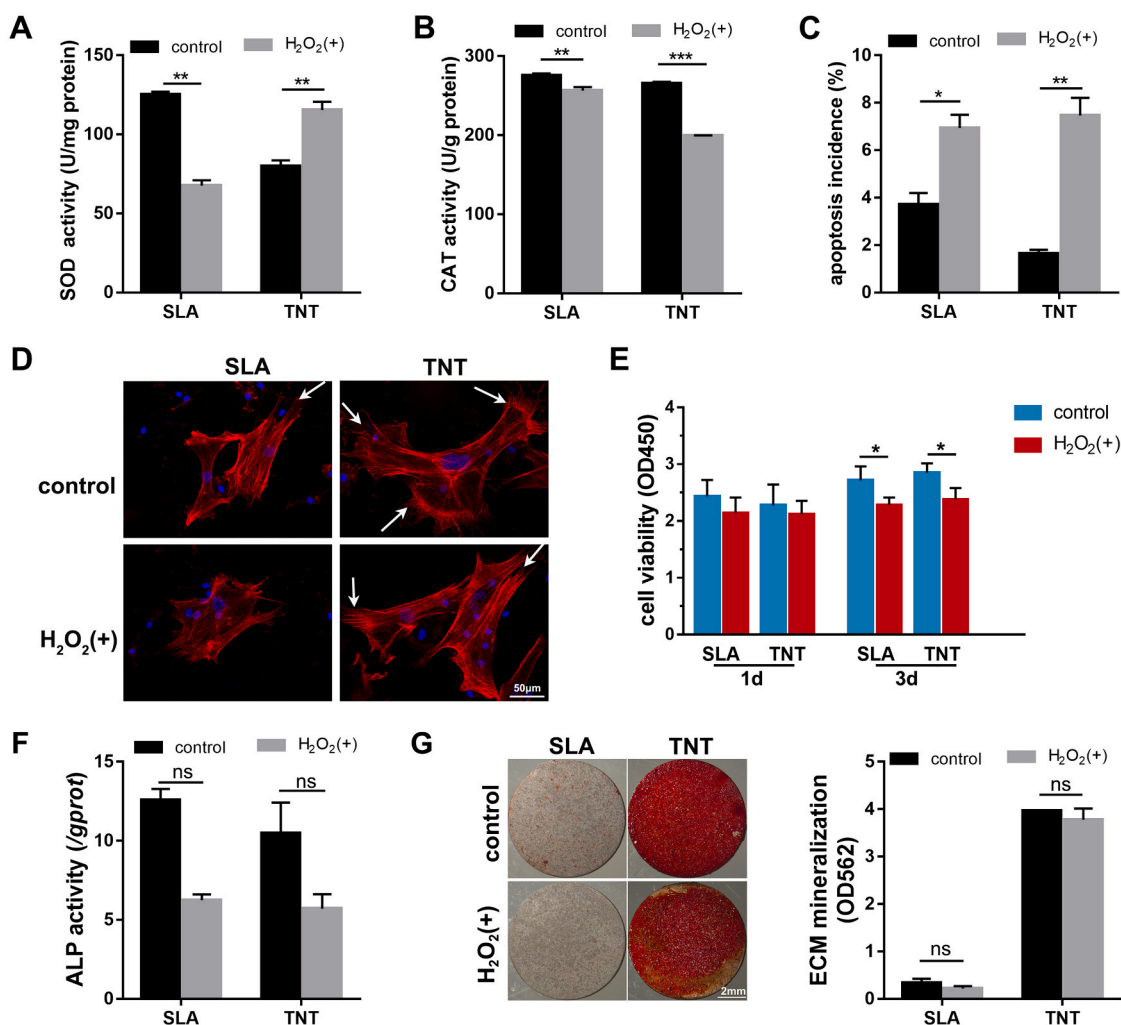


Fig. 3. TNT enhanced oxidation resistance and osteogenic differentiation of MSCs under H₂O₂-induced oxidative stress. (A–C) SOD and CAT activity (A&B) and apoptosis incidence (C) of MSCs on 2 Ti surfaces after exposure to H₂O₂ for 1 day. (D&E) Adhesion (D) and proliferation (E) of MSCs on 2 Ti surfaces after exposure to H₂O₂ for 1 and 3 d. The white arrows mark lamellipodia. (F–G) The ALP activity (F) and ECM mineralization (G) of MSCs on 2 Ti surfaces under H₂O₂-induced oxidative stress after osteogenic induction for 7 and 21 d, respectively. **p* < 0.05, ***p* < 0.01, ****p* < 0.001, ns indicates no significant difference.

To evaluate the effect of oxidative stress on the biological behavior of MSCs on Ti surfaces, adhesion, proliferation and osteogenic differentiation, including ALP viability and mineralization levels, were measured. The fluorescence staining of F-actin showed that the MSCs stretched out in several directions on TNT covering a larger area than SLA under normal conditions (Fig. 3D). After exposure to H₂O₂ for 24 h, the MSCs still spread fully with apparent lamellipodia despite being oriented in a single direction on TNT, while the adhesion of MSCs shrank obviously on SLA. For cell proliferation, the effect of substrates and H₂O₂ on the proliferation of MSCs was not obvious on the first day of stimulation. After exposure to H₂O₂ for 3 d, the proliferation of MSCs was significantly suppressed on both substrates in a trend of a slight increase compared with that on day 1. In addition, the proliferation level of MSCs on TNTs was slightly higher than that on SLAs regardless of the culture conditions (Fig. 3E).

Regarding the effect of oxidative stress on osteogenic differentiation, the ALP activity of MSCs was reduced by approximately half under oxidative stress conditions, while there was no significant difference between SLA and TNT on day 7 of osteogenic induction (Fig. 3F). After osteogenic induction for 14 d, TNT induced a much higher level of mineralization of MSCs under both normal and oxidative stress conditions than SLA (Fig. 3G). Under LPS-induced oxidative stress, the mineralization level was maintained at a higher level on TNT than the

prohibited level on SLA (Fig. S3B), despite the enhanced ALP activity upon stimulation with LPS (Fig. S3A). The results indicated that the early phase of osteogenesis was more susceptible to oxidative stress, while the inhibitory effect of H₂O₂ faded in the late stage of osteogenesis. In general, TNT induced a higher level of osteogenesis regardless of the culture conditions.

3.4. FoxO1 silencing abolished the oxidation resistance and osteogenic superiority of MSCs on TNTs under oxidative stress

To reveal the molecular mechanism of antioxidation on TNT, the expression levels of typical signaling proteins in MSCs were measured. The expression of the autophagy marker LC3II, the oxidation-defense-related transcription factor FoxO1 and downstream targets, including SOD2 and CAT, was activated in the presence of oxidative stress. In addition, relatively higher levels of these proteins were expressed in MSCs cultured on TNT under oxidative stress (Fig. 4A&S4A).

To elaborate the contribution of FoxO1 to the oxidation resistance and osteogenic superiority of MSCs in TNT under oxidative stress, the transcription factor FoxO1 was silenced using a shRNA lentiviral vector. After silencing FoxO1 in MSCs, ROS production was elevated in MSCs on SLA and TNT (Fig. 4C). Similarly, increased apoptosis rates in the early phase (*p* < 0.05) were detected on both SLA and TNT despite the lack of

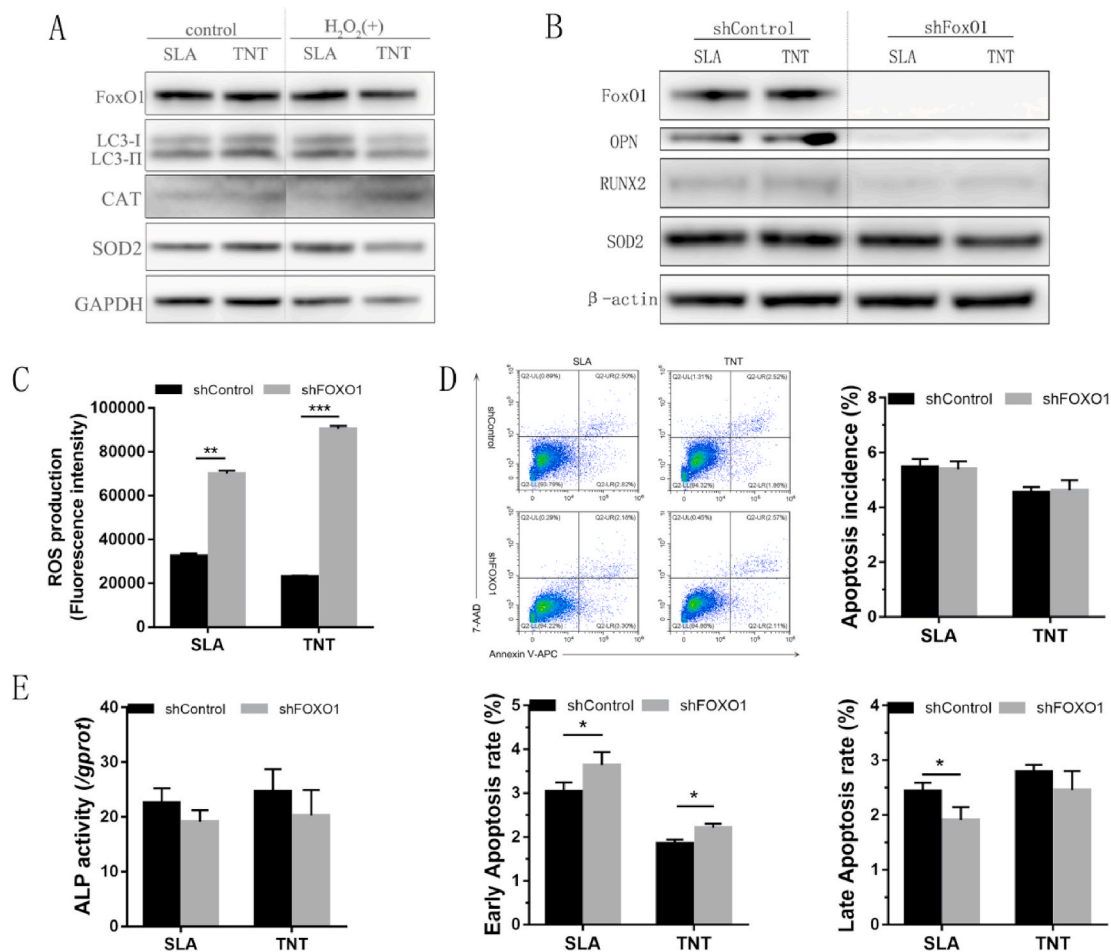


Fig. 4. FoxO1 silencing abolished the oxidation resistance and osteogenic superiority of MSCs on TNTs under oxidative stress. (A) Expression profiles of signaling proteins, including foxO1, LC3-I/LC3-II, CAT, and SOD2, in MSCs on 2 Ti surfaces after culture with/without 300 μM H_2O_2 for 24 h. (B–F) MSCs transduced with shFoxO1 or shControl were cultured on 2 Ti surfaces with 300 μM H_2O_2 , and the expression levels of osteogenic proteins and the antioxidant SOD2 (B), intracellular ROS (C), apoptotic incidence (D), and ALP activity (E) after osteogenic induction for 7days were determined. * $p < 0.05$, ** $p < 0.01$, *** $p < 0.001$.

a significant change in total apoptosis incidence (Fig. 4D). Regarding the osteogenic capacity of MSCs, the ALP activity of MSCs was slightly decreased on titanium surfaces after FoxO1 was silenced (Fig. 4E). However, silencing FoxO1 inhibited the expression of osteogenic proteins, including OPN and Runx2, as well as the antioxidant SOD2, to similar levels on the 2 titanium surfaces (Fig. 4B&S4B). Together, the results indicated that FoxO1 promoted the expression of antioxidants, therefore restraining ROS production and apoptosis and promoting osteogenic differentiation on titanium surfaces under oxidative stress.

3.5. TNT alleviated oxidative stress and skewed the inflammatory response toward anti-inflammatory extremities under oxidative stress compared with SLA

To determine how M ϕ s on Ti surfaces survived redox regulation under H_2O_2 -mediated oxidative stress, the expression levels of antioxidant enzymes were measured. For the activity of antioxidant enzymes, no significant change was observed among the SOD activities of RAW264.7 cells on different Ti surfaces or under different culture conditions (Fig. S5A). However, the CAT activity of macrophages on both surfaces was impaired by H_2O_2 . Even so, the CAT activity of macrophages on TNTs remained higher than that on SLAs under oxidative stress (Fig. S5B). Furthermore, M ϕ s cultured on TNTs generally exhibited a similar expression pattern of signaling proteins as MSCs under oxidative stress, with higher levels of FoxO1 in TNTs and comparable levels of CAT with SLAs (Figs. S5C–G).

As oxidative stress is closely related to inflammation, the inflammatory response of macrophages was also evaluated. The results of immunofluorescence in the H_2O_2 -mediated model revealed that macrophages cultured on the 2 surfaces were activated upon stimulation with H_2O_2 , as indicated by the increased percentages of both M1 (iNOS positive) and M2 (CD163 positive) phenotypes. However, more macrophages adhered to TNTs polarized to M2 macrophages than to SLAs, although M1 macrophages outnumbered M2 macrophages under oxidative stress in a general manner (Fig. 5A&D). In the LPS-mediated inflammatory model, macrophages were activated upon stimulation with LPS, with stretched pseudopodia (Fig. S6A&B), increased expression of iNOS and decreased expression of CD163 (Fig. 5B&E, S6C&D). Similarly, although the expression of the M2 marker CD163 was lower under hyperglycemia than under normal conditions, the proportion of M2 macrophages was relatively higher in TNTs than in SLAs (Fig. 5C&F). Overall, the results revealed that compared with SLA, TNT alleviated oxidative stress and skewed the polarization of macrophages to the M2 phenotype under oxidative stress.

Additionally, the expression and secretion of inflammatory cytokines by M ϕ s and MSCs on Ti surfaces were detected. An inflammatory cytokine microarray demonstrated that a mild inflammatory response was initiated upon stimulation of H_2O_2 in M ϕ s adhered to titanium surfaces, but cascade reactions were initiated in both M ϕ s and MSCs under LPS-activated inflammatory conditions (Fig. 6A&B, S7). Specifically, macrophages on TNT secreted fewer proinflammatory cytokines, including TNF- α and IL-6, and more anti-inflammatory

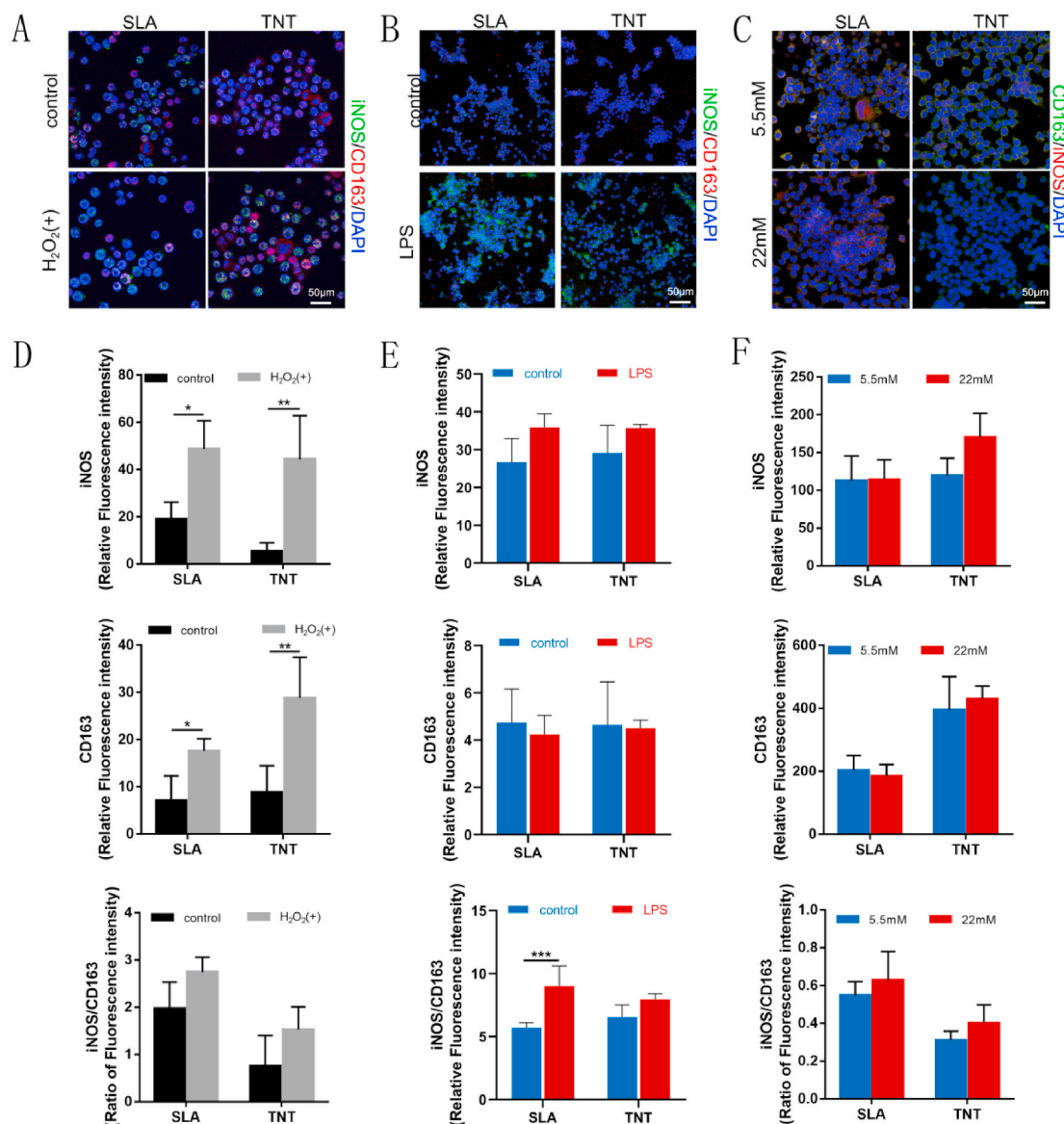


Fig. 5. TNT alleviated oxidative stress and skewed the polarization of macrophages to the M2 phenotype under oxidative stress. Confocal images of M1 and M2 macrophage markers iNOS and CD163 expressed in Mφs on 2 Ti surfaces under H₂O₂- (A), LPS- (B), and hyperglycemia- (C) mediated oxidative stress and corresponding semiquantitative analysis (D–F). **p* < 0.05, ***p* < 0.01, ****p* < 0.001.

cytokines, especially IL-10, than those on SLA in the presence of H₂O₂ (Fig. 6C). For the LPS-mediated TNT model, the mRNA expression of M1 macrophage markers (CD86, iNOS, TNF-α, IL-18) increased after stimulation with LPS, while there was no significant change in M2 macrophage markers, including CD206 and IL-10 (Fig. S6E), consistent with the protein secretion of inflammatory cytokines. In addition, TNT induced lower secretion levels of proinflammatory cytokines, including INF-γ and IL-6, from both Mφs and MSCs than SLA under LPS stimulation (Fig. S7). However, high glucose appeared to suppress the expression of inflammatory cytokines, while more IL-10 was still expressed on TNTs (Fig. 6D), similar to the pattern in the H₂O₂-derived model. Taken together, the results suggested that under oxidative stress, TNT can skew the inflammatory response of macrophages and MSCs toward the anti-inflammatory extremity.

3.6. TNT exhibited superior osteoimmunomodulatory activity under oxidative stress

As both MSCs and macrophages aggregate at the interface of

implants and surrounding bone, it is essential to understand the cross-talk between these two types of cells. Under H₂O₂-induced oxidative stress, TNTs exhibited higher osseoinnunity capacity in the later phase of osteogenic differentiation, as indicated by higher ECM mineralization than SLAs (Fig. 7A–C). Further investigation of osseoinnunity regulation of TNT showed that the inhibition of ALP activity of MSCs on TNT by oxidative stress was aggravated to a significant level by the supernatants from H₂O₂-treated macrophages (Fig. 7F). However, the ECM mineralization of MSCs was significantly suppressed by H₂O₂ regardless of the addition of the supernatants from H₂O₂-treated macrophages (Fig. 7G). LPS also inhibited the osteogenesis of MSCs on TNTs in a similar temporal-dependent pattern (Fig. S8). The results indicated that macrophages aggravated the suppressive effect of oxidative stress on the early osteogenic differentiation of MSCs, but not at the later stage. In general, TNTs exhibited higher osseoinnunity capacity in the later phase of osteogenic differentiation under oxidative stress.

In turn, MSCs can also play an immunomodulatory role in macrophages. The H₂O₂-induced increase in TNF-α and IL-6 secretion was significantly ameliorated by cocultured MSCs (Fig. 7H and I), indicating

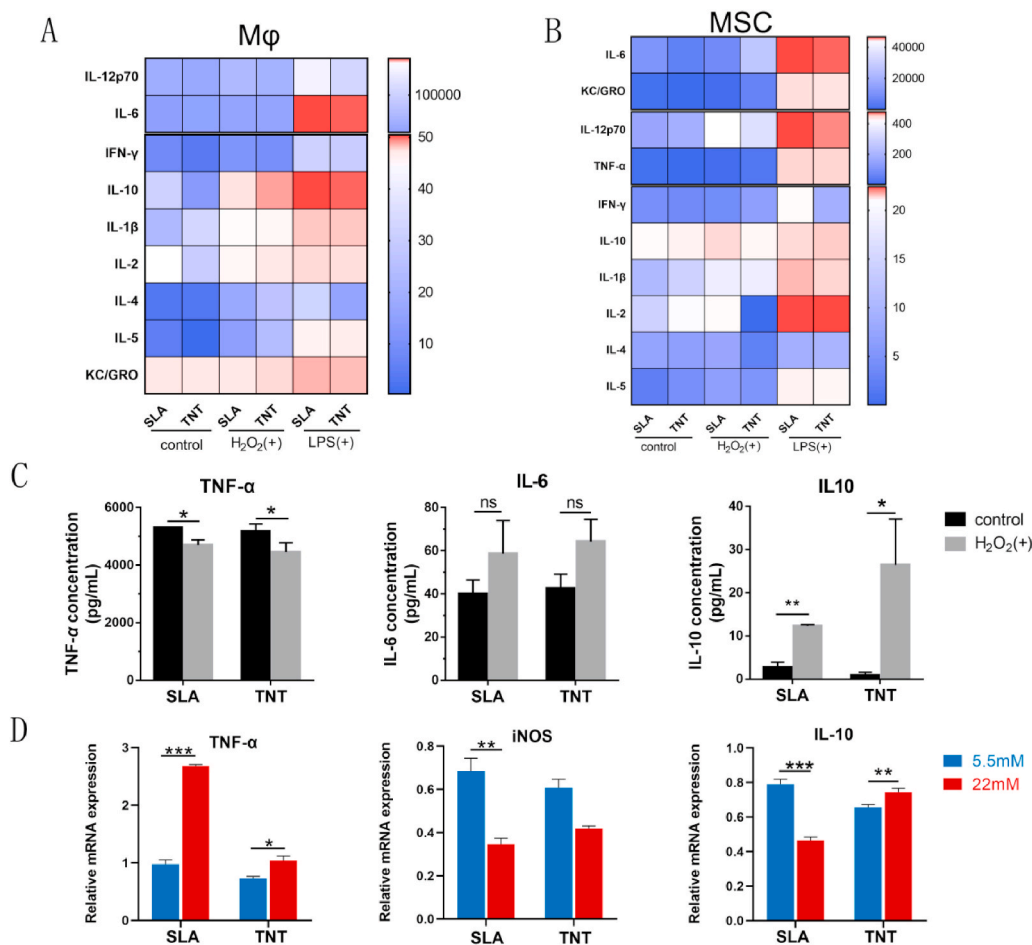


Fig. 6. TNT skewed the profiles of inflammatory cytokines toward anti-inflammatory extremities under oxidative stress compared with SLA. (A&B) Microarray of inflammatory cytokines secreted by Mφs and MSCs cultured on 2 Ti surfaces under H₂O₂ and LPS stimulation. A mild inflammatory response was initiated upon stimulation of H₂O₂ in Mφs adhered to 2 Ti surfaces, but a cascade reaction was initiated in both Mφs and MSCs under LPS-activated inflammatory conditions. (C) Detailed comparison of inflammatory cytokines secreted by Mφs adhered to 2 titanium surfaces under H₂O₂-induced oxidative stress. (D) The mRNA expression profiles of inflammatory cytokines from macrophages on 2 Ti surfaces under hyperglycemic conditions. **p* < 0.05, ***p* < 0.01, ****p* < 0.001.

that MSCs can negatively regulate the inflammatory response of Mφs in a paracrine manner.

3.7. TNT facilitated the osteointegration of implants, oxidation resistance and the anti-inflammatory response in diabetic rats

Rats with type 1 diabetes were used as an animal model of oxidative stress corroborated by elevated oxidative stress indexes, including serum MDA levels and urine 8-OHdG excretion (Fig. 8A&B).

To evaluate the osteointegration of SLA and TNT implants with micro/nanotopographies, VG staining to indicate bone tissue was performed. New bone developed around the implants after implantation in the femurs for 4 weeks (Fig. 8C). Generally, more blue-stained fibrous tissue was observed in the DM group, leading to a lower BIC% than that in the control group (Fig. 8D). Of note, neonatal bone around TNT implants was more compact than that around SLA implants in normal rats. Moreover, new bone grew into the gaps between the TNT implant thread in diabetic rats, resulting in a higher BIC% and an alleviated decline in BIC% compared with SLA (Fig. 8E). At week 8, the peri-implant bone became stronger, but the compact bone in DM rats was thinner than that in contemporary normal rats, accompanied by fibrous tissue remaining in the bone-implant interface, which was rarely observed in normal rats (Fig. 8C). Collectively, TNT mitigated the compromised osteointegration of implants in diabetic rats.

Immunohistochemical staining showed that the levels of oxidation products of DNA and lipids, 8-OHdG and 4-HNE, in peri-implant bone tissue were reduced by TNT in diabetic rats compared with SLA (*p* < 0.05), despite the lack of a significant difference between normal and diabetic rats (Fig. S9). In contrast, inflammatory response initiation was insufficient in the peri-implant tissues of diabetic rats compared with

normal rats, consistent with the inactive expression of inflammatory cytokines under hyperglycemia-induced cellular oxidative stress. Furthermore, less TNF-α was distributed in the integratedlyhealing adjacent tissue of diabetic rats around the TNT than in the SLA. Meanwhile, IL-10 was expressed at comparable levels in peri-implant tissues of TNT and SLA (Fig. S10).

4. Discussion

In the current study, nanoscale TiO₂ nanotube coatings on titanium implants exhibited superior osteogenesis and osseointegration compared with microscale SLA under oxidative stress, attributed to their FoxO1-induced antioxidant properties and anti-inflammatory osteoimmunity.

It has been widely established that oxidative stress plays a critical role in the pathogenesis and complications of aging and aging-related and metabolic diseases such as osteoporosis, osteoarthritis, and diabetes mellitus and impairs the process of osseogenesis [5,24,25]. Thus, it is essential to study the bioadaptation of bone implants to oxidative stress and the relevant mechanism to guide the future development of implants for the aging population [3]. Aside from pathological conditions that exist prior to material implantation, oxidative stress can also derive from inflammation that exists in the biological reaction after material-tissue contact [10]. Therefore, it is a prerequisite to construct heterogeneous models of oxidative stress to comprehensively evaluate the bioactivity and bioadaptation of biomaterials, while a unitary model has been adopted in most existing research [26–28]. Accordingly, H₂O₂ and LPS were used to simulate inherent and inflammation-mediated cellular models of oxidative stress. Specifically, the effect of hyperglycemia-induced oxidative stress on osseoimmunity was further

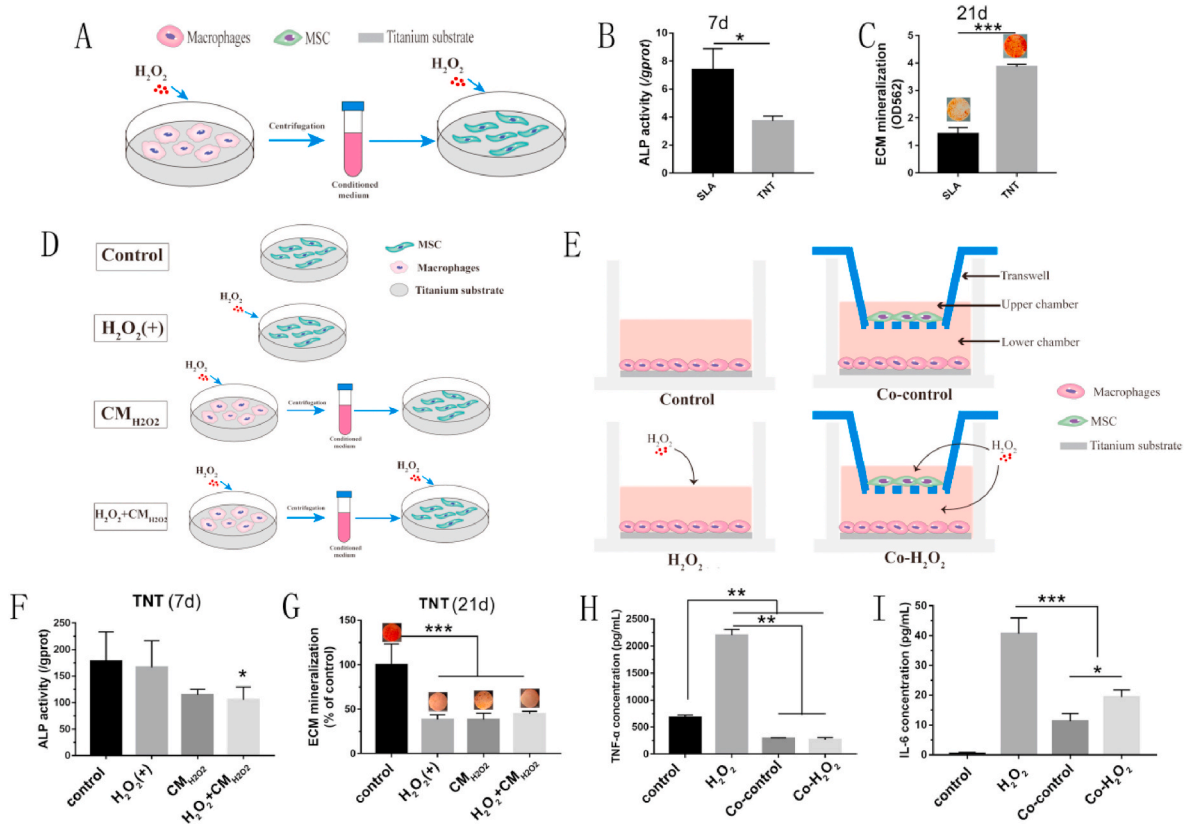


Fig. 7. TNT exhibited superior osteoimmunomodulatory activity under oxidative stress. (A–C) Conditioned medium from Mφs on different Ti surfaces was collected to culture MSCs on corresponding surfaces (A), and then the ALP activity (B) and ECM mineralization (C) of MSCs cultivated on different conditioned media were evaluated for 7 and 21 d, respectively. (D&E) Grouping diagram showing different modes of MSC-Mφ coculture on TNTs. (F&G) The ALP activity (F) and mineralization (G) of MSCs cultivated on the surface of TNTs in various media according to the diagram in (D) were evaluated for 7 and 21 d, respectively. (H&I) The secretion levels of TNF-α and IL6 from RAW264.7 cells with different culture patterns according to diagram (E) were measured on the TNT surface. **p* < 0.05, ***p* < 0.01, ****p* < 0.001.

explored, extending our latest study [17]. Among diverse cellular models of oxidative stress [29–31], H₂O₂-induced oxidative stress is the classic model, covering most circumstances of oxidative stress and is therefore adopted as the major model in the current study. However, there is no canonical animal model of oxidative stress because oxidative stress is more of a concept defined as an imbalance between oxidants and antioxidants extracted from multifarious pathological conditions *in vivo* [9, 32]. Cu and Zn superoxide dismutase (SOD1) knockout animals, diabetes mellitus, osteoporosis, osteoarthritis and other aging-related diseases are all candidate models [33]. As a major risk factor in implant therapy impairing osteointegration [34], diabetes mellitus was adopted as the *in vivo* model of oxidative stress in the current study. Higher levels of hallmarks of systematic oxidative stress [17], serum MDA and urine 8-OHdG in type 1 diabetes rats also justified the option of diabetes as an animal model of oxidative stress.

Oxidative stress in diverse models was found to trigger ROS production, induce cell apoptosis and suppress osteogenic differentiation of MSCs adhered to titanium surfaces in the present study and our previous research on the impact of hyperglycemia on osteoblasts [17] as well as most research [35,36]. However, this negative impact could be alleviated in MSCs adhered to TNT due to the antioxidative capacity, accompanied by relieved impairment of osseointegration in diabetic rats compared with SLA. The surface physical and chemical properties of biomaterials, such as topography and wettability, can alter the redox state by modulating cell adhesion and cytoskeletal reorganization. Takeshi's study found that ultraviolet (UV) light treatment induced the superhydrophilicity of titanium and inhibited ROS production in osteoblasts adhered to the UV-treated titanium surface [37]. Consistently, in

the current study, it was found that TNT presented low roughness and superhydrophilicity, which facilitated MSC attachment and induced antioxidant capacity compared with SLA. One of the potential mechanisms of increased antioxidant properties on TNT is activation of the nuclear factor-E2-related factor 2(Nrf2)/Kelch-like ECH-associated protein 1 (Keap1)–antioxidant response element (ARE) signaling pathway. Keap1 binds to the actin cytoskeleton and functions as a sensor for mechanical force [38]. The physicochemical alteration of substrate surfaces transfers mechanical stimuli to the cytoskeleton and influences the Nrf2-Keap1 interaction. Upon activation by oxidative stress, Nrf2 translocates into the nucleus and binds to AREs, promoting the transcription of a wide variety of antioxidant genes [39]. Another potential mechanism is the Rho/Rho-kinase (ROCK) signaling pathway, which can modulate actin cytoskeleton organization in response to oxidative stress [40,41]. It was reported that activating Rho signaling partially restored the cell stiffness destroyed by oxidative stress and decreased the intracellular ROS level [42]. Accordingly, TNT may promote MSC adhesion via the Rho/ROCK pathway, which further interferes with the redox state. These hypotheses may explain why TNT could neutralize ROS, although future studies are needed to verify the hypotheses.

The underlying mechanism of enhanced osteogenesis was inspired by the observation that MSCs on TNT express higher levels of FoxO1 and antioxidants, including SOD2 and CAT. Thus, it is hypothesized that FoxO1 induces TNT oxidation-resistance induction by upregulating the expression of antioxidants and subsequently mitigates the inhibitory effect of ROS on osteogenesis. This hypothesis was corroborated by FoxO1 loss-of-function experiments, in which oxidation resistance and osteogenesis promotion effects were reversed. Similarly, Yonglin Yu

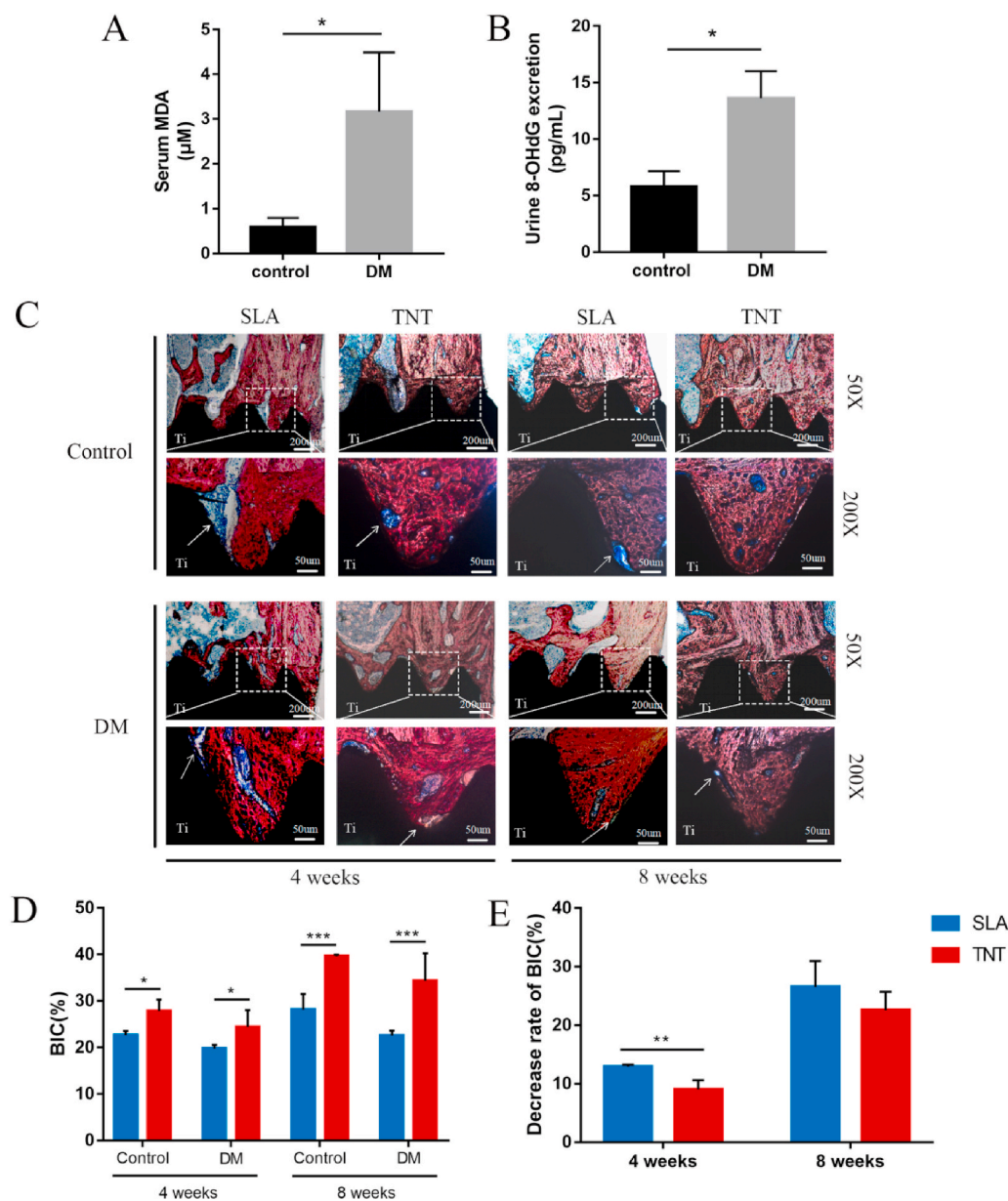


Fig. 8. TNT mitigated compromised osteointegration of implants in diabetic-related oxidative stress rats. (A&B) Systematic oxidative stress levels, including urine 8-OHdG excretion and serum MDA levels, were measured in DM and normal rats. **(C)** Histological staining of hard tissue sections after implantation in the DM rat model for 4 and 8 weeks. The newly formed bone was stained red, while the fibrous tissues were stained blue, and implants were stained black. **(D)** Analysis of the percentages of bone-implant contact (BIC%) after 4 and 8 weeks of implantation. **(E)** The decrease rates of BIC%. * $p < 0.05$, ** $p < 0.01$, *** $p < 0.001$. There was no significant difference between the two groups without *.

et al. also employed H₂O₂ (300 mM)-incorporating medium to create an oxidative environment in osteoblasts and found that large TNT samples (110 nm in diameter) demonstrated superior cellular behaviors under oxidative stress [36]. However, they ascribed the superior cellular behaviors to the increased phosphorylation level of another FOXO transcription factor – FOXO3a – resulting in blocking its inhibitory effect on osteogenic differentiation. These seemingly contradictory findings are intelligible on the basis that the role of the foxO family in bone formation under oxidative stress remains controversial and paradoxical, although it has been extensively explored [43,44]. Multiple upstream pathways regulate FOXO activity, resulting in diverse downstream effects on their function as homeostasis regulators to maintain tissue homeostasis [12]. Even in the process of osteogenic differentiation, the regulation of FOXO is cell-specific and phase-dependent. In line with our finding that FoxO1 upregulated the expression of OPN and Runx2, FoxO1 was confirmed to directly target the Runx2 gene and act as a positive upstream regulator of Runx2 throughout differentiation [13]. The results suggested that the regulatory function of FOXO was carefully explored in a specific context.

As the core component of the adaptive immune system residing in the peri-implant bone microenvironment, macrophages can also be shaped by different titanium micro/nanotextures [14] and can exhibit different patterns of inflammatory responses. As canonical inflammatory stimuli for M1-like macrophages [10], LPS triggers a cascade of inflammatory cytokines, especially proinflammatory species, in macrophages. In such an inflammatory milieu, different immune microenvironments consisting of diverse inflammatory cytokine profiles can still be distinguished on titanium surfaces with different topographies, exhibiting different bioadaptations [45]. Macrophages on TNTs secrete fewer proinflammatory cytokines, including INF- γ and IL-6, under LPS stimulation, thus breaking or alleviating the positive feedback loops on the activation of M1-like macrophages. Macrophages can also be activated by H₂O₂ but induce a mild inflammatory response, in accordance with chronic, low-grade inflammation characterized by aging and age-related diseases [5,46,47]. In this scenario, the inflammatory response of macrophages on TNTs was skewed toward anti-inflammatory extremities, with a higher ratio of M2 to M1 macrophages and notable secretion of IL-10. This advantage was relevant to

activated FoxO1 in macrophages, a canonical cytoprotective mechanism against oxidative injury and a regulator of inflammatory pathways [48]. A similar activation pattern was observed in high glucose-induced oxidative stress, facilitating later osteogenesis verified by *in vitro* osteoimmunology experiments and the positive relationship between the initial inflammation phase and later osteogenesis *in vivo* in current research [49,50]. However, compared with the direct impact of oxidative stress on MSCs, macrophages further repressed MSC osteogenesis via amplification of upregulated reactive oxygen species in an LPS-mediated model, which contradicts Luo's study [51]. The reason for the divergence may lie in the different targeted conditions: oxidative stress conditions in our study and normal conditions in Luo's study. The results highlighted the significant role of circumstances in the crosstalk between macrophages and mesenchymal stem cells.

5. Conclusion

In summary, heterogeneous models of oxidative stress simulating various pathological conditions were formulated in the current study. Under such settings, nanoscale TNT coatings on titanium implants exhibited superior osteogenesis and osseointegration compared with microscale SLA surfaces, ascribed to FoxO1-induced oxidation resistance and anti-inflammatory osteoimmunity. This study not only suggests the potential application of TiO₂ nanotube coatings on titanium implants in populations suffering from bone degenerative disease but also provides a systematic evaluation strategy for the future development of bone implant biomaterials.

CRediT authorship contribution statement

Jingyan Huang: Conceptualization, Methodology, Formal analysis, Investigation, Data curation, Writing – original draft, Writing – review & editing, Project administration. **Ruoqi Li:** Validation, Formal analysis, Investigation, Writing – review & editing. **Jinghong Yang:** Formal analysis, Investigation. **Min Cai:** Investigation. **Yichen Lee:** Investigation. **Anxun Wang:** Conceptualization, Methodology. **Bin Cheng:** Supervision, Visualization. **Yan Wang:** Methodology, Supervision, Funding acquisition, Writing – review & editing.

Declaration of competing interest

The authors declare that they have no known competing financial interests or personal relationships that could have appeared to influence the work reported in this paper.

Acknowledgments

The authors would like to thank Zhipei Chen for the assistance with this project. This work was supported by the Guangdong Financial Fund for High-Caliber Hospital Construction (174-2018-XMZC-0001-03-0125/D-09, China) and the Guangdong Basic and Applied Basic Research Foundation (2019A1515011842, 2020A1515010291, China).

Appendix A. Supplementary data

Supplementary data to this article can be found online at <https://doi.org/10.1016/j.bioactmat.2021.02.023>.

References

- [1] H.N.S. Almassri, Y. Ma, Z. Dan, Z. Ting, Y. Cheng, X. Wu, Implant stability and survival rates of a hydrophilic versus a conventional sandblasted, acid-etched implant surface: systematic review and meta-analysis, *J. Am. Dent. Assoc.* 151 (2020) 444–453, <https://doi.org/10.1016/j.adaj.2020.03.002>.
- [2] V. Moraschini, L.A. Poubel, V.F. Ferreira, S. Barboza Edos, Evaluation of survival and success rates of dental implants reported in longitudinal studies with a follow-up period of at least 10 years: a systematic review, *Int. J. Oral Surg.* 44 (2015) 377–388, <https://doi.org/10.1016/j.ijom.2014.10.023>.
- [3] H.S. Alghamdi, J.A. Jansen, The development and future of dental implants, *Dent. Mater.* J. 39 (2020) 167–172, <https://doi.org/10.4012/dmj.2019.140>.
- [4] T. Finkel, N.J. Holbrook, Oxidants, Oxidative stress and the biology of ageing, *Nature* 408 (2000) 239–247, <https://doi.org/10.1038/35041687>.
- [5] B. Yu, C.Y. Wang, Osteoporosis: the result of an 'aged' bone microenvironment, *Trends Mol. Med.* 22 (2016) 641–644, <https://doi.org/10.1016/j.molmed.2016.06.002>.
- [6] D.A. Butterfield, B. Halliwell, Oxidative stress, dysfunctional glucose metabolism and Alzheimer disease, *Nat. Rev. Neurosci.* 20 (2019) 148–160, <https://doi.org/10.1038/s41583-019-0132-6>.
- [7] I. Liguori, G. Russo, F. Curcio, G. Bulli, L. Aran, D. Della-Morte, G. Gargiulo, G. Testa, F. Cacciatore, D. Bonaduce, P. Abete, Oxidative stress, aging, and diseases, *Clin. Interv. Aging* 13 (2018) 757–772, <https://doi.org/10.2147/CIA.S158513>.
- [8] G. Murdolo, D. Bartolini, C. Tortoioli, M. Piroddi, P. Torquato, F. Galli, Selenium and cancer stem cells, *Adv. Canc. Res.* 136 (2017) 235–257, <https://doi.org/10.1016/bs.acr.2017.07.006>.
- [9] F. Ursini, M. Maiorino, H.J. Forman, Redox homeostasis: the Golden Mean of healthy living, *Redox Biol* 8 (2016) 205–215, <https://doi.org/10.1016/j.redox.2016.01.010>.
- [10] P.A. MOUTHUY, S.J.B. Snelling, S.G. Dakin, L. Milkovic, A.C. Gasparovic, A.J. Carr, N. Zarkovic, Biocompatibility of implantable materials: an oxidative stress viewpoint, *Biomaterials* 109 (2016) 55–68, <https://doi.org/10.1016/j.biomaterials.2016.09.010>.
- [11] L. Knani, D. Bartolini, S. Kechiche, C. Tortoioli, G. Murdolo, M. Moretti, I. Messaoudi, R.J. Reiter, F. Galli, Melatonin prevents cadmium-induced bone damage: first evidence on an improved osteogenic/adipogenic differentiation balance of mesenchymal stem cells as underlying mechanism, *J. Pineal Res.* 67 (2019), e12597, <https://doi.org/10.1111/jpi.12597>.
- [12] A. Eijkelenboom, B.M. Burgering, FOXOs: signalling integrators for homeostasis maintenance, *Nat. Rev. Mol. Cell Biol.* 14 (2013) 83–97, <https://doi.org/10.1038/nrm3507>.
- [13] D. Chen, Y. Gong, L. Xu, M. Zhou, J. Li, J. Song, Bidirectional regulation of osteogenic differentiation by the FOXO subfamily of Forkhead transcription factors in mammalian MSCs, *Cell Prolif* 52 (2019), e12540, <https://doi.org/10.1111/cpr.12540>.
- [14] Z. Chen, T. Klein, R.Z. Murray, R. Crawford, J. Chang, C. Wu, Y. Xiao, Osteoimmunomodulation for the development of advanced bone biomaterials, *Mater. Today* 19 (2016) 304–321, <https://doi.org/10.1016/j.mat.2015.11.004>.
- [15] Z. Chen, A. Bachhuka, S. Han, F. Wei, S. Lu, R.M. Visalakshan, K. Vasilev, Y. Xiao, Tuning chemistry and topography of nanoengineered surfaces to manipulate immune response for bone regeneration applications, *ACS Nano* 11 (2017) 4494–4506, <https://doi.org/10.1021/acsnano.6b07808>.
- [16] J. Huang, X. Zhang, W. Yan, Z. Chen, X. Shuai, A. Wang, Y. Wang, Nanotubular topography enhances the bioactivity of titanium implants, *Nanomed. Nanotechnol. Biol. Med.* 13 (2017) 1913–1923, <https://doi.org/10.1016/j.nano.2017.03.017>.
- [17] J. Yang, H. Zhang, S. Chan, R. Li, Y. Wu, M. Cai, A. Wang, Y. Wang, TiO₂ nanotubes alleviate diabetes-induced osteogenic inhibition, *Int. J. Nanomed.* 15 (2020) 3523–3537, <https://doi.org/10.2147/IJN.S237008>.
- [18] H. Zhu, Z.K. Guo, X.X. Jiang, H. Li, X.Y. Wang, H.Y. Yao, Y. Zhang, N. Mao, A protocol for isolation and culture of mesenchymal stem cells from mouse compact bone, *Nat. Protoc.* 5 (2010) 550–560, <https://doi.org/10.1038/nprot.2009.238>.
- [19] P.A. Alvarado-Vazquez, L. Bernal, C.A. Paige, R.L. Grosick, C. Moracho-Vilrriales, D. W. Ferreira, C. Ulecia-Moron, E.A. Romero-Sandoval, Macrophage-specific nanotechnology-driven CD163 overexpression in human macrophages results in an M2 phenotype under inflammatory conditions, *Immunobiology* 222 (2017) 900–912, <https://doi.org/10.1016/j.imbio.2017.05.011>.
- [20] N. Percie du Sert, V. Hurst, A. Ahluwalia, S. Alam, M.T. Avey, M. Baker, W. J. Browne, A. Clark, I.C. Cuthill, U. Dirnagl, M. Emerson, P. Garner, S.T. Holgate, D.W. Howells, N.A. Karp, S.E. Lazic, K. Lidster, C.J. MacCallum, M. Macleod, E. J. Pearl, O.H. Petersen, F. Rawle, P. Reynolds, K. Rooney, E.S. Sena, S. D. Silberberg, T. Steckler, H. Wurbel, The ARRIVE guidelines 2.0: updated guidelines for reporting animal research, *PLoS Biol.* 18 (2020), e3000410, <https://doi.org/10.1371/journal.pbio.3000410>.
- [21] C. Hollands, The Animals (scientific procedures) Act 1986, *Lancet* 2 (1986) 32–33, [https://doi.org/10.1016/s0140-6736\(86\)92571-7](https://doi.org/10.1016/s0140-6736(86)92571-7).
- [22] S. Hayashi, T. Nakamura, Y. Motooka, F. Ito, L. Jiang, S. Akatsuka, A. Iwase, H. Kajiyama, F. Kikkawa, S. Toyokuni, Novel ovarian endometriosis model causes infertility via iron-mediated oxidative stress in mice, *Redox Biol* 37 (2020) 101726, <https://doi.org/10.1016/j.redox.2020.101726>.
- [23] L. Liu, Y. Wu, Q. Li, J. Liang, Q. He, L. Zhao, J. Chen, M. Cheng, Z. Huang, H. Ren, J. Chen, L. Peng, F. Gao, D. Chen, A. Wang, METTL3 promotes tumorigenesis and metastasis through BMI1 m(6)A methylation in oral squamous cell carcinoma, *Mol. Ther.* 28 (2020) 2177–2190, <https://doi.org/10.1016/j.yjmt.2020.06.024>.
- [24] J. Luo, K. Mills, S. le Cessie, R. Noordam, D. van Heemst, Ageing, age-related diseases and oxidative stress: what to do next? *Ageing Res. Rev.* 57 (2020) 100982, <https://doi.org/10.1016/j.arr.2019.100982>.
- [25] F. Giacco, M. Brownlee, Oxidative stress and diabetic complications, *Circ. Res.* 107 (2010) 1058–1070, <https://doi.org/10.1161/CIRCRESAHA.110.223545>.
- [26] M.A. Fouda, M.R. Ghovanloo, P.C. Ruben, Cannabidiol protects against high glucose-induced oxidative stress and cytotoxicity in cardiac voltage-gated sodium channels, *Br. J. Pharmacol.* 177 (2020) 2932–2946, <https://doi.org/10.1111/bph.15020>.

- [27] H. Wu, Y. Wang, Y. Zhang, F. Xu, J. Chen, L. Duan, T. Zhang, J. Wang, F. Zhang, Breaking the vicious loop between inflammation, oxidative stress and coagulation, a novel anti-thrombus insight of nattokinase by inhibiting LPS-induced inflammation and oxidative stress, *Redox Biol* 32 (2020) 101500, <https://doi.org/10.1016/j.redox.2020.101500>.
- [28] C. Wen, J.X. Zhang, Y.Q. Feng, Y.Q. Duan, H.L. Ma, H.H. Zhang, Purification and identification of novel antioxidant peptides from watermelon seed protein hydrolysates and their cytoprotective effects on H₂O₂-induced oxidative stress, *Food Chem.* 327 (2020) 127059, <https://doi.org/10.1016/j.foodchem.2020.127059>.
- [29] X. Wu, H. Dai, L. Liu, C. Xu, Y. Yin, J. Yi, M.D. Bielec, Y. Han, S. Li, Citrate reduced oxidative damage in stem cells by regulating cellular redox signaling pathways and represent a potential treatment for oxidative stress-induced diseases, *Redox. Biol.* 21 (2019) 101057, <https://doi.org/10.1016/j.redox.2018.11.015>.
- [30] M. Mashimo, J. Kato, J. Moss, ADP-ribosyl-acceptor hydrolase 3 regulates poly (ADP-ribose) degradation and cell death during oxidative stress, *Proc. Natl. Acad. Sci. U.S.A.* 110 (2013) 18964–18969, <https://doi.org/10.1073/pnas.1312783110>.
- [31] S.B. Iloki-Assanga, L.M. Lewis-Lujan, D. Fernandez-Angulo, A.A. Gil-Salido, C. L. Lara-Espinoza, J.L. Rubio-Pino, Retino-protective effect of *Bucida buceras* against oxidative stress induced by H₂O₂ in human retinal pigment epithelial cells line, *BMC Compl. Alternative Med.* 15 (2015) 254, <https://doi.org/10.1186/s12906-015-0765-6>.
- [32] H. Sies, On the history of oxidative stress: concept and some aspects of current development, *Curr. Opin. Toxicol.* 7 (2018) 122–126, <https://doi.org/10.1016/j.cotox.2018.01.002>.
- [33] Y.D. Bai, Y.R. Yang, X.P. Mu, G. Lin, Y.P. Wang, S. Jin, Y. Chen, M.J. Wang, Y. C. Zhu, Hydrogen sulfide alleviates acute myocardial ischemia injury by modulating autophagy and inflammation response under oxidative stress, *Oxid. Med. Cell. Longevity.* 2018 (2018) 3402809, <https://doi.org/10.1155/2018/3402809>.
- [34] F. Javed, G.E. Romanos, Chronic hyperglycemia as a risk factor in implant therapy, *Periodontol* 81 (2019) (2000) 57–63, <https://doi.org/10.1111/prd.12283>.
- [35] F. Atashi, A. Modarressi, M.S. Pepper, The role of reactive oxygen species in mesenchymal stem cell adipogenic and osteogenic differentiation: a review, *Stem Cell. Dev.* 24 (2015) 1150–1163, <https://doi.org/10.1089/scd.2014.0484>.
- [36] Y. Yu, X. Shen, Z. Luo, Y. Hu, M. Li, P. Ma, Q. Ran, L. Dai, Y. He, K. Cai, Osteogenesis potential of different titania nanotubes in oxidative stress microenvironment, *Biomaterials* 167 (2018) 44–57, <https://doi.org/10.1016/j.biomaterials.2018.03.024>.
- [37] T. Ueno, T. Ikeda, N. Tsukimura, M. Ishijima, H. Minamikawa, Y. Sugita, M. Yamada, N. Wakabayashi, T. Ogawa, Novel antioxidant capability of titanium induced by UV light treatment, *Biomaterials* 108 (2016) 177–186, <https://doi.org/10.1016/j.biomaterials.2016.08.050>.
- [38] M.I. Kang, A. Kobayashi, N. Wakabayashi, S.G. Kim, M. Yamamoto, Scaffolding of Keap1 to the actin cytoskeleton controls the function of Nrf2 as key regulator of cytoprotective phase 2 genes, *Proc. Natl. Acad. Sci. U.S.A.* 101 (2004) 2046–2051, <https://doi.org/10.1073/pnas.0308347100>.
- [39] B. Chen, Y. Lu, Y. Chen, J. Cheng, The role of Nrf2 in oxidative stress-induced endothelial injuries, *J. Endocrinol.* 225 (2015) R83–R99, <https://doi.org/10.1530/JOE-14-0662>.
- [40] M.P. Girouard, M. Pool, R. Alchini, I. Rambaldi, A.E. Fournier, RhoA proteolysis regulates the actin cytoskeleton in response to oxidative stress, *PLoS One* 11 (2016), e0168641, <https://doi.org/10.1371/journal.pone.0168641>.
- [41] R. Patel, S. Sriramoji, M. Marucci, I. Aziz, S. Shah, F. Sesti, Cytoskeletal remodeling via Rho GTPases during oxidative and thermal stress in *Caenorhabditis elegans*, *Biochem. Biophys. Res. Commun.* 492 (2017) 338–342, <https://doi.org/10.1016/j.bbrc.2017.08.112>.
- [42] S. Sun, S. Wong, A. Mak, M. Cho, Impact of oxidative stress on cellular biomechanics and rho signaling in C2C12 myoblasts, *J. Biomech.* 47 (2014) 3650–3656, <https://doi.org/10.1016/j.jbiomech.2014.09.036>.
- [43] L. Liao, X. Su, X. Yang, C. Hu, B. Li, Y. Lv, Y. Shuai, H. Jing, Z. Deng, Y. Jin, TNF- α inhibits FoxO1 by upregulating miR-705 to aggravate oxidative damage in bone marrow-derived mesenchymal stem cells during osteoporosis, *Stem Cell.* 34 (2016) 1054–1067, <https://doi.org/10.1002/stem.2274>.
- [44] M. Almeida, L. Han, M. Martin-Millan, C.A. O'Brien, S.C. Manolagas, Oxidative stress antagonizes Wnt signaling in osteoblast precursors by diverting beta-catenin from T cell factor- to forkhead box O-mediated transcription, *J. Biol. Chem.* 282 (2007) 27298–27305, <https://doi.org/10.1074/jbc.M702811200>.
- [45] Y. Wang, Bioadaptability: an innovative concept for biomaterials, *J. Mater. Sci. Technol.* 32 (2016) 801–809, <https://doi.org/10.1016/j.jmst.2016.08.002>.
- [46] W. Sendama, The effect of ageing on the resolution of inflammation, *Ageing Res. Rev.* 57 (2020) 1010000, <https://doi.org/10.1016/j.arr.2019.101000>.
- [47] H.Y. Chung, D.H. Kim, E.K. Lee, K.W. Chung, S. Chung, B. Lee, A.Y. Seo, J. H. Chung, Y.S. Jung, E. Im, J. Lee, N.D. Kim, Y.J. Choi, D.S. Im, B.P. Yu, Redefining chronic inflammation in aging and age-related diseases: proposal of the senoinflammation concept, *Aging. Dis.* 10 (2019) 367–382, <https://doi.org/10.14336/AD.2018.0324>.
- [48] L. Virag, R.I. Jaen, Z. Regdon, L. Bosca, P. Prieto, Self-defense of macrophages against oxidative injury: fighting for their own survival, *Redox. Biol.* 26 (2019) 101261, <https://doi.org/10.1016/j.redox.2019.101261>.
- [49] X. Yuan, H. Cao, J. Wang, K. Tang, B. Li, Y. Zhao, M. Cheng, H. Qin, X. Liu, X. Zhang, Immunomodulatory effects of calcium and strontium Co-doped titanium oxides on osteogenesis, *Front. Immunol.* 8 (2017) 1196, <https://doi.org/10.3389/fimmu.2017.01196>.
- [50] R. Lin, C. Deng, X. Li, Y. Liu, M. Zhang, C. Qin, Q. Yao, L. Wang, C. Wu, Copper-incorporated bioactive glass-ceramics inducing anti-inflammatory phenotype and regeneration of cartilage/bone interface, *Theranostics* 9 (2019) 6300–6313, <https://doi.org/10.7150/thno.36120>.
- [51] M.L. Luo, Y. Jiao, W.P. Gong, Y. Li, L.N. Niu, F.R. Tay, J.H. Chen, Macrophages enhance mesenchymal stem cell osteogenesis via down-regulation of reactive oxygen species, *J. Dent.* 94 (2020) 103297, <https://doi.org/10.1016/j.jdent.2020.103297>.